

Resonant tunneling in a quantum waveguide: Effect of a finite-size attractive impurity

Chang Sub Kim

Department of Physics, Chonnam National University, Kwangju 500-757, Korea

Arkady M. Satanin

Department of Theoretical Physics, Nizhny Novgorod University, Nizhny Novgorod 603091, Russia

Yong S. Joe and Ronald M. Cosby

Department of Physics and Astronomy, Ball State University, Muncie, Indiana 47306-0505

(Received 12 November 1998; revised manuscript received 5 May 1999)

We investigate the electron transport in a quasi-one-dimensional constriction with an attractive, finite-size impurity, in the ballistic limit theoretically. Within the envelope function approximation we formulate the scattering matrix exactly that determines the resonance structure of the electron transmission. Due to the multiple impurity levels under the many-channel conditions, multiple Breit-Wigner resonances and Fano line shapes appear in the same energy window. By varying the size of the impurity, we predict novel coherent effects such as the collapse of the Fano resonance and antiresonance, resonance-level inversion, and the appearance of discrete levels in the continuum. [S0163-1829(99)07439-1]

I. INTRODUCTION

The discovery of conductance quantization has motivated a great deal of research interests in the quantum transport phenomena in semiconductor nanostructures.^{1,2} In particular, the effect of disorder on the electron transmission caused by elastic scattering with impurities in the narrow constrictions has been investigated intensively in recent years both theoretically and experimentally.³⁻¹⁷ The presence of impurities in such size-quantized systems or *quantum waveguides* opens up new possibilities of taming electronic states and provides a basis for further study of coherent quantum effects. It was shown that a single impurity changes the shape of the conductance quantization dramatically, giving rise to erosion of the ideal quantum plateau. In order to understand the mechanisms of the conductance erosion, several model potentials were proposed for the impurity: the point-impurity model,⁶ the model potential having lateral extension,⁸ and the finite-size impurity model.¹⁷

In this paper, we study the resonance structures of the electron transmission in a quantum waveguide with a finite-size scatterer for a wide range of the impurity parameters. The quantum waveguide considered is a quasi-one-dimensional (Q1D) constriction and a rectangular attractive square well is used to represent the impurity potential. We strictly limit our attention to the electron transport in the ballistic limit other than the impurity scattering and to the case of zero-magnetic field. Although we treat the popular model, our work is distinguishable from the previous investigations in several aspects. First of all, we present the formally exact expression for the transmission amplitude within the envelope function approximation. Secondly, we analyze the Fano asymmetric resonance structures that appear in addition to the usual Breit-Wigner line shapes in our system. Although a similar feature of Fano structures for a finite-size impurity model was treated in Ref. 6, we provide here much details. Also, the model study in Ref. 17 did not recognize

the possible appearance of Fano resonances due to the restriction of the energy window considered. Third, we predict some novel coherent phenomena such as the collapse of Fano resonances, the inversion of resonance levels, and the creation of discrete levels embedded in the continuum. The fundamental parameters of an impurity might be extracted from the analysis of the resonant structure of conductance in real systems. Also, the class of coherent resonant phenomena predicted may emerge in experiments by tailoring the impurity potential using the modern nanolithography techniques.

In the quantum waveguide, the transverse eigenfunctions, specifying the energy subbands, play the role of an infinite number of independent channels for longitudinal electron motion. Depending on the incident electron energy E , some channels are opened and others are closed for electron propagation through the waveguide. We analyze the transmission amplitudes $t_{nn'}(E)$ that characterize the electron scattering from channel n' to n as the electron goes through the quantum waveguide. The transmission amplitudes as analytic functions of the energy E provide useful information on the system. The poles are connected with bound or quasibound states and their lifetimes. Also, the two-probe conductance of the system can be obtained from $t_{nn'}(E)$ through the Landauer-Büttiker formula.^{18,19} We will present the results for the electron transmission $T(E)$, calculated by summing the transmission amplitudes over all the *open* channels,

$$T(E) = \sum_{nn'} \frac{k_n}{k_{n'}} |t_{nn'}|^2 \equiv \sum_{nn'} T_{nn'}, \quad (1)$$

where k_n is the electron wave vector of channel n . For the finite-size impurity model considered in this paper, multiple impurity levels appear. Consequently, the intriguing coherent resonant effects are induced under the multichannel condition in the electron transmission. We obtain physically different Breit-Wigner resonances and Fano resonances in the same energy window and analyze, in particular, the behavior

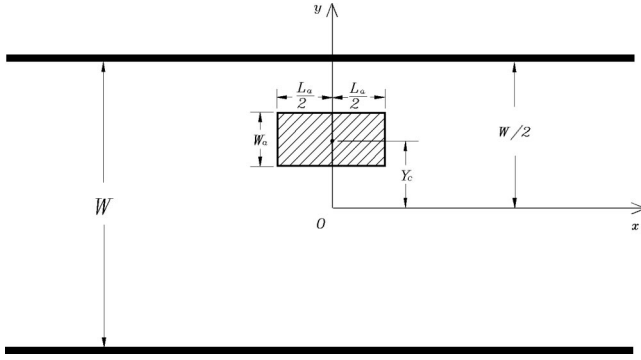


FIG. 1. Schematic diagram of the quantum waveguide for electron transmission containing an attractive rectangular impurity. The center of the impurity is chosen to be at $(0, Y_c)$, i.e., shifted from the center of the waveguide.

of the Fano structures in detail to study the effects of the spatial extension of the impurity on the transmission. In addition, we predict the possibility of the electron confinement in the space occupied by the finite-size impurity. It is shown that the predicted localized electron states are degenerate with the scattering states at the special energies and the impurity sizes.

The paper is organized as follows. In Sec. II, we define the finite-size impurity model and derive the formally exact expression for the scattering matrix for the electron transmission. As an illustration of the formula obtained in Sec. II, the exact result for an effective 1D model system is given in Sec. III. Section IV is devoted to the detailed analysis of the effect of the finite-size impurity on the electron transmission. In Sec. V, the interesting electron confinement situation is discussed. Finally, we summarize our results in Sec. VI. The extremely short-ranged impurity is considered in Appendix A as a limiting case as well as the point-impurity model.

II. FORMULATION

We consider the electron transmission through a Q1D quantum waveguide of width W , containing a finite-size attractive impurity, which is depicted in Fig. 1 schematically. It is assumed that the waveguide is infinitely long and is placed along the x direction. The confinement potential in the transverse direction is modeled by the potential $V_c(y)$ and the impurity potential is represented by the function $V(x, y)$.

Within an effective mass approximation, the electron wave function in the waveguide is determined by the Schrödinger equation

$$-\frac{\hbar^2}{2m^*} \left(\frac{\partial^2}{\partial x^2} + \frac{\partial^2}{\partial y^2} \right) \Psi(x, y) + V_c(y) \Psi(x, y) + V(x, y) \Psi(x, y) = E \Psi(x, y), \quad (2)$$

where m^* is the effective mass of the electron. We attempt to find the electron wave function in the expansion form

$$\Psi(x, y) = \sum_{n=1}^{\infty} \psi_n(x) \varphi_n(y), \quad (3)$$

where, for instance, use can be made of a simple choice of an infinite square well for the confinement potential $V_c(y)$ to define the complete basis

$$\varphi_n(y) = \sqrt{\frac{2}{W}} \sin \left[\frac{n\pi}{W} \left(y + \frac{W}{2} \right) \right], \quad (4)$$

where $n=1, 2, \dots$, whose corresponding eigenenergies are $E_n = \hbar^2 \pi^2 n^2 / (2m^* W^2)$. Substituting Eq. (3) into Eq. (2) we find the equation for $\psi_n(x)$ as

$$-\frac{\hbar^2}{2m^*} \frac{\partial^2}{\partial x^2} \psi_n(x) + \sum_{n'=1}^{\infty} V_{nn'}(x) \psi_{n'}(x) = (E - E_n) \psi_n(x), \quad (5)$$

where the matrix elements are defined to be

$$V_{nn'}(x) \equiv \int dy \varphi_n(y) V(x, y) \varphi_{n'}(y). \quad (6)$$

We adopt the two-dimensional rectangular well model for the impurity potential,¹⁷ which is described by

$$V(x, y) = -V_{att} F(x) G(y - Y_c), \quad (7)$$

where V_{att} is the depth of the quantum well and the center of impurity is assumed to be located at $x=0$ and $y=Y_c$. The functions $F(x)$ and $G(y)$ are defined to give unity when $|x| \leq L_a/2$ and $|y| \leq W_a/2$, respectively, otherwise zero. Then, the wave functions in Eq. (3) are written in each region as

$$\Psi(x, y) = \sum_n [A_n e^{ik_n(x+L_a/2)} + B_n e^{-ik_n(x+L_a/2)}] \varphi_n(y), \quad \text{for } x \leq -L_a/2, \quad (8)$$

$$\Psi(x, y) = \sum_n [a_n e^{iq_n x} + b_n e^{-iq_n x}] \chi_n(y), \quad \text{for } -L_a/2 \leq x \leq L_a/2, \quad (9)$$

$$\Psi(x, y) = \sum_n C_n e^{ik_n(x-L_a/2)} \varphi_n(y), \quad \text{for } x \geq L_a/2, \quad (10)$$

where $k_n = \sqrt{2m^*(E - E_n)}/\hbar$ and $q_n = \sqrt{2m^*(E - E_n^{tr})}/\hbar$ are the longitudinal components of the wave vectors outside and inside of the impurity region, respectively. And, $\chi_n(y)$ and E_n^{tr} are the eigenfunctions and the energy levels of an electron in the transverse field $V_{tr}(y)$,

$$V_{tr}(y) = -V_{att} G(y - Y_c) + V_c(y). \quad (11)$$

Two sets of eigenfunctions φ_n and χ_n are connected by the unitary matrix U ,

$$U_{nn'} = \int dy \varphi_n(y) \chi_{n'}(y). \quad (12)$$

Note that solutions with real k_n and q_n are the propagating states, whereas for imaginary $k_n = i|k_n|$ or $q_n = i|q_n|$, evanescent modes are the corresponding solutions.

Next, by examining the continuity conditions of the wave functions and their derivatives at $x = \pm L_a/2$, one can find the

equations for the amplitudes A_n , B_n , a_n , b_n , and C_n . Here, we present only the results in matrix form,

$$\begin{aligned} \mathbf{d}^{-1}\mathbf{a} + \mathbf{d}\mathbf{b} &= \mathbf{U}(\mathbf{A} + \mathbf{B}), \\ \mathbf{q}(\mathbf{d}^{-1}\mathbf{a} - \mathbf{d}\mathbf{b}) &= \mathbf{U}\mathbf{k}(\mathbf{A} - \mathbf{B}), \\ \mathbf{d}\mathbf{a} + \mathbf{d}^{-1}\mathbf{b} &= \mathbf{U}\mathbf{C}, \\ \mathbf{q}(\mathbf{d}\mathbf{a} - \mathbf{d}^{-1}\mathbf{b}) &= \mathbf{U}\mathbf{k}\mathbf{C}, \end{aligned} \quad (13)$$

where we have defined

$$(\mathbf{k})_{nn'} = k_n \delta_{nn'}, \quad (\mathbf{q})_{nn'} = q_n \delta_{nn'}, \quad (\mathbf{d})_{nn'} = e^{i\theta_n} \delta_{nn'}. \quad (14)$$

In the above $\theta_n \equiv q_n L_a / 2$ is the phase of the electron wave and the wave amplitudes \mathbf{a} , \mathbf{b} , \mathbf{A} , \mathbf{B} , and \mathbf{C} are considered as infinite vectors. After eliminating the intermediate amplitudes \mathbf{a} and \mathbf{b} in Eq. (13), it is possible to find the scattering matrix \mathbf{t} that is defined through

$$\mathbf{C} = \mathbf{t}\mathbf{A}.$$

The result is

$$\mathbf{t} = \mathbf{M}^{-1} = \frac{\mathbf{M}_C^T}{\det(\mathbf{M})}, \quad (15)$$

where \mathbf{M}_C is the cofactor of the matrix \mathbf{M} , which is defined to be

$$\begin{aligned} \mathbf{M} &= \frac{1}{4} \mathbf{U}^{-1} [(\mathbf{1} + \hat{\mathbf{k}}^{-1} \mathbf{q}) \mathbf{D}^{-1} (\mathbf{1} + \mathbf{q}^{-1} \hat{\mathbf{k}}) \\ &\quad + (\mathbf{1} - \hat{\mathbf{k}}^{-1} \mathbf{q}) \mathbf{D} (\mathbf{1} - \mathbf{q}^{-1} \hat{\mathbf{k}})] \mathbf{U}, \end{aligned} \quad (16)$$

where $\hat{\mathbf{k}} = \mathbf{U}\mathbf{k}\mathbf{U}^{-1}$, $\mathbf{D} = \mathbf{d}^2$, and $\mathbf{1}$ is the unit matrix. Equation (15) suggests that the analytic properties of the transmission amplitude as a function of energy are fully determined by the structure of the matrix \mathbf{M} . The resonance states follow from the poles of the matrix \mathbf{M} , specified by

$$\det(\mathbf{M}) = 0, \quad (17)$$

and the zero energies at which the transmission quenches are determined by

$$[\mathbf{M}_C]_{nn'} = 0, \quad n, n' = 1, 2, \dots \quad (18)$$

The reflection symmetry of the impurity potential with respect to $x \rightarrow -x$ allows us to carry out the factorization, $\mathbf{M} = \mathbf{U}^{-1} \mathbf{M}_a \mathbf{M}_s \mathbf{U}$, with definitions

$$\mathbf{M}_s = \frac{1}{2} [-(\mathbf{d} - \mathbf{d}^{-1}) + (\mathbf{d} + \mathbf{d}^{-1}) \mathbf{q}^{-1} \hat{\mathbf{k}}]$$

and

$$\mathbf{M}_a = \frac{1}{2} [-(\mathbf{d} - \mathbf{d}^{-1}) + \hat{\mathbf{k}} \mathbf{q}^{-1} (\mathbf{d} + \mathbf{d}^{-1})].$$

Hence, Eq. (17) can be decoupled into two equations: one for symmetric resonance states,

$$\det(\mathbf{M}_s) = 0, \quad (19)$$

and the other for antisymmetric resonance states,

$$\det(\mathbf{M}_a) = 0. \quad (20)$$

III. AN EXACT RESULT

As an illustration of the utility of our formulation described in Sec. II, we consider here a simple model defined by setting $W_a \equiv W$ that allows an exact solution to Eq. (15). Since, in this case, the transverse eigenfunction χ_n is identical to φ_n with only a shift of eigenenergy, $E_n^{tr} = E_n - V_{att}$, we have $\mathbf{U} = \mathbf{1}$ from Eq. (12). Then, Eq. (16) becomes

$$\begin{aligned} (\mathbf{M})_{nn'} &= \frac{1}{4} \left[\left(1 + \frac{q_n}{k_n} \right) \left(1 + \frac{k_n}{q_n} \right) e^{-2i\theta_n} \right. \\ &\quad \left. + \left(1 - \frac{q_n}{k_n} \right) \left(1 - \frac{k_n}{q_n} \right) e^{2i\theta_n} \right] \delta_{nn'}. \end{aligned} \quad (21)$$

Accordingly, the scattering amplitude $t_{nn'}$ turns out to be diagonal from Eq. (15) and is obtained exactly as

$$t_{nn}(E) = \frac{4k_n q_n}{(q_n + k_n)^2 e^{-2i\theta_n} - (q_n - k_n)^2 e^{2i\theta_n}}. \quad (22)$$

This model corresponds physically to the situation of having noninteracting channels. Thus, the problem is essentially reduced to a one-dimensional system without mixing among different n 's. One can quickly notice that $t_{nn}(E_n) = 0$: the transmission vanishes identically for the incident electron wave φ_n at the subband minimum $E = E_n$. Poles that specify symmetric and antisymmetric resonance states are determined by

$$\tan \theta_n = -ik_n/q_n \quad \text{and} \quad \cot \theta_n = ik_n/q_n, \quad (23)$$

respectively. There exist two types of poles, depending on the incident electron energy. For energies $E > E_n$, the poles are placed in the complex energy plane and the resonance is characterized by the Breit-Wigner line shape,

$$t_{nn}(E) = \frac{i\gamma_{nj}}{E - \tilde{E}_{nj} + i\gamma_{nj}}, \quad (24)$$

where

$$\tilde{E}_{nj} = E_n - V_{att} + \left(\frac{\pi}{L_a} \right)^2 \frac{\hbar^2 j^2}{2m^*} \quad \text{and} \quad \gamma_{nj} = \frac{2\hbar^2}{m^* L_a} k_n(\tilde{E}_{nj})$$

with $j = 1, 2, 3, \dots$. On the other hand, when the electron is transmitted into the waveguide through the channel φ_n with an energy E limited by $E_n - V_{att} < E < E_n$, the poles are located on the real energy axis. This means that the corresponding resonance states are discrete levels, located below E_n .

IV. FINITE-SIZE IMPURITY

It is well known that the asymmetric resonance structures appear in the transmission for the extremely short-ranged impurity model.^{13,15,20} Such a Fano line shape consists of a paired, asymmetric resonance peak and nearby transmission zero and can be represented by [see Appendix A]

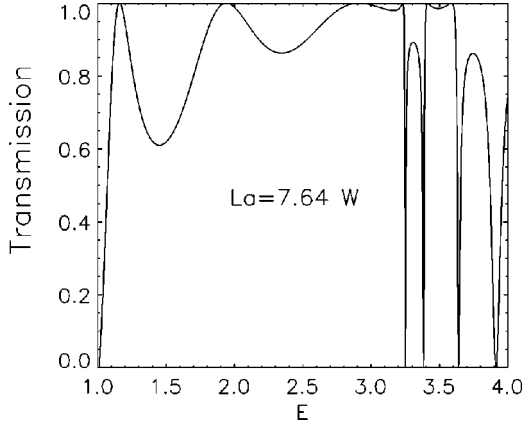


FIG. 2. Transmission through the electron waveguide with the finite-size impurity along the propagation direction as a function of the incident energy E in the first energy window (E_1, E_2) where E is in units of E_1 ; we have used $V_{att} = 6.37 E_1$, $W_a = 0.1 W$, $L_a = 7.64 W$, and $Y_c = -0.17 W$.

$$t(E) \sim \frac{E - E_0}{E - E_R + i\Gamma}, \quad (25)$$

where E_0 is the zero energy, E_R is the location of the asymmetric peak, and Γ specifies the half width of the quasibound state.²¹ This resonance is due to the interaction of the bound-level raised in the continuum with the continuum states. The relaxation of the short-range interaction limit, namely the use of a finite-size scatterer along the propagation direction, would produce multiple impurity levels, that could change the transmission dramatically. It is expected that a nontrivial interaction between such levels and the continuum under the multichannel condition gives rise to a novel resonant structure in the transmission. For atomic systems this kind of interaction was investigated to observe the effect of resonance overlapping.²²

To reduce the calculational efforts without losing the desired aspects, we impose the condition $W_a \ll L_a$, leading to the short-ranged transverse potential

$$V_{tr}(y) = -\frac{\hbar^2 u}{m^*} \delta(y - Y_c) + V_c(y), \quad (26)$$

where $u \equiv m^* V_{att} W_a / \hbar^2$. The corresponding eigenvalues E_n^{tr} are obtained by

$$\sin(\kappa W) = 2 \frac{u}{\kappa} \sin(\kappa Y_c) \sin[\kappa(W - Y_c)], \quad (27)$$

where $\kappa \equiv \sqrt{2m^*E/\hbar^2}$, as derived from the transverse Schrödinger equation. When the interaction is turned off ($u=0$), one recovers the eigenfunctions Eq. (4) and eigenvalues E_n . In the general case ($u \neq 0$), we have solved Eq. (27) numerically and the first few eigenvalues are

$$E_1^{tr} = -0.60 E_1, \quad E_2^{tr} = 3.19 E_1, \quad \text{and} \quad E_3^{tr} = 8.99 E_1.$$

We have also obtained the corresponding eigenfunctions $\chi_n(y)$, not presented here. The common parameters used in this section are

$$m^* = 0.067 m_e, \quad V_{att} = 6.37 E_1,$$

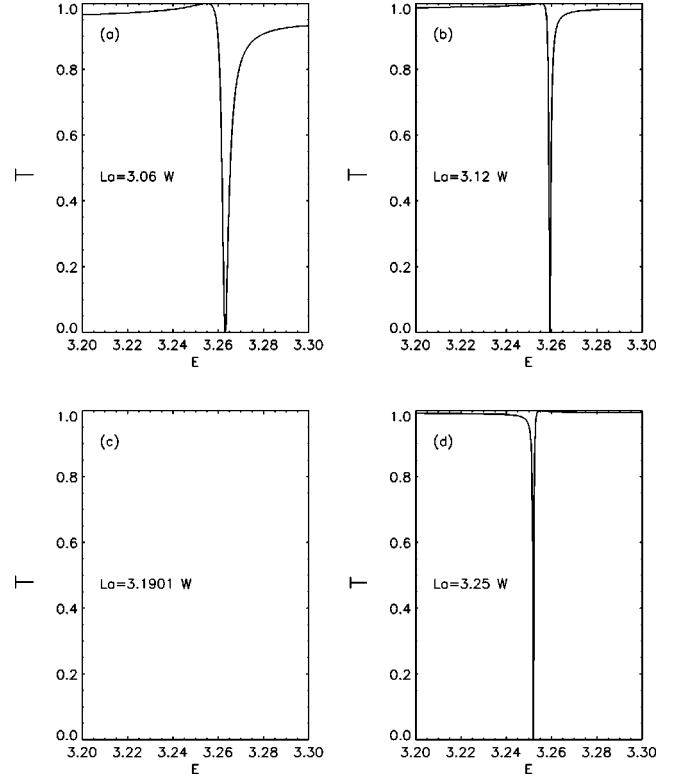


FIG. 3. Transmission as a function of energy E near the first impurity sizes: (a) $L_a = 3.06 W$, (b) $L_a = 3.12 W$, (c) $L_a = 3.1901 W$, and (d) $L_a = 3.25 W$; where no curve is exhibited in (c) since $T=1$ over the energies shown, thus overlapping with the top axis. [Precise $T=1$ occurs only at $E=E_c$.] The other parameters are the same as in Fig. 2.

$$W_a = 0.1 W, \quad \text{and} \quad Y_c = -0.17 W.$$

In the following, we report the full numerical results obtained by calculating the transmission matrix Eq. (15) and thus by evaluating the transmissivity Eq. (1), while restricting our attention to the energy interval (E_1, E_2) .

In Fig. 2 we present a representative case where very interesting transmission lines show up: the Lorentzian Breit-Wigner resonances appear in lower energies $E_1 < E < E_2^{tr}$, whereas the multiple asymmetric Fano lines appear in the upper energies $E_2^{tr} < E < E_2$. The Breit-Wigner peaks occur at $E \doteq 1.15, 1.96,$ and $2.90 E_1$ and the half width of each resonance specifies the lifetime of the corresponding quasibound state. The asymmetric Fano peaks are seen to occur at $E \doteq 3.22, 3.40,$ and $3.58 E_1$ and the Fano dips, in this case the transmission zeros, are seen to occur at $E \doteq 3.24, 3.37, 3.63,$ and $3.90 E_1$. The Breit-Wigner resonances are associated with the interference of the electron waves with the geometrical structure of the finite-size impurity. The multiple Fano resonances are connected with the interaction of the multiple quasidonor levels appearing above the lowest subband edge and the continuum states, of which detailed analysis will be given later. It is of interest to see that the Fano resonance dominates the resonance structure in the region where it overlaps with the Breit-Wigner line. We estimated that the line width $\gamma \sim 0.79 E_1$ for the Breit-Wigner resonance at $E \sim 2.91 E_1$ and the Fano width $\Gamma \sim 0.6 \times 10^{-2} E_1$

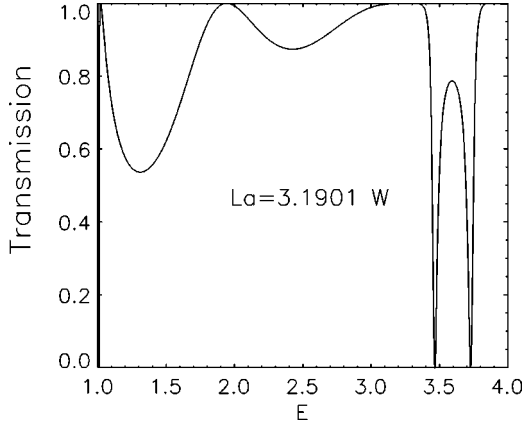


FIG. 4. Transmission as a function of E in the full first energy window (E_1, E_2) where $L_a = 3.1901 W$ has been used, corresponding to Fig. 3(c). The other parameters are the same as in Fig. 2.

at $E \sim 3.215 E_1$ in Fig. 2. Accordingly, the ratio $\Gamma/\gamma \sim 0.8 \times 10^{-2}$, meaning that the Breit-Wigner pole is placed far away from the real energy axis to bring small influence on the resonance structure.

Next, we vary the size of the impurity (L_a) in order to investigate its effect on the transmission. In Fig. 3, we depict the transmission near a Fano resonance-antiresonance for various sizes of the impurity, $L_a = 3.06, 3.12, 3.1901$, and $3.25 W$. We have chosen the energy region near the first Fano line in Fig. 2. The result shows two important new features. First, as the impurity length reaches a special value $L_a = 3.1901 W \equiv L_c$, the Fano structure disappears, giving rise to full transmission over the energy range considered [Fig. 3(c)]. This collapse of Fano resonance and antiresonance is seen more clearly in Fig. 4 where we plot the transmission in the entire first energy window: the energy region around $E \sim 3.255 E_1 \equiv E_c$ admits the full transmission. Secondly, the location of the Fano pole is switched with the zero energy as L_a goes through the special distance L_c . Namely, the resonance peak occurs before the transmission zero when $L_a < L_c$, Figs. 3(a) and 3(b), but it occurs after the transmission zero when $L_a > L_c$, Fig. 3(d). The observed *inversion* of the resonance level seems quite a novel effect in the transmission problem, of which physical interpretation is given below.

It is intriguing to understand the numerically observed collapse of Fano structures and inversion of resonance peaks.

TABLE I. Critical impurity sizes and energy levels for symmetric states; where L_c and E_c are in units of W and E_1 , respectively.

j	$\alpha(j)$	$L_c(\alpha(j))$	$E_c(\alpha(j))$
1	0.9233	1.0982	3.4798
2	1.1743	2.1507	3.3104
3	1.2825	3.1901	3.2551
4	1.3439	4.2246	3.2306
5	1.3836	5.2563	3.2177
\vdots	\vdots	\vdots	\vdots
∞	$\pi/2$	∞	E_2^*/E_1

To this end, we present here the analytical manipulation for the resonance-amplitude. It suffices to consider the resonantly coupled two channels ($n=1$ and 2) in the energy interval, $E_2^* < E < E_2$, in the weak-coupling limit. Note that both channels are propagating modes in the region $|x| < L_a/2$ with the wave vectors q_1 and q_2 , but outside the impurity region, $|x| > L_a/2$, only mode $n=1$ is propagating with k_1 while mode $n=2$ being the evanescent wave with $k_2 = i|k_2|$. Accordingly, the transmission is specified by $t_{11}(E)$, whose shape near a Fano structure is described by Eq. (25). Our detailed analysis of Eq. (17) shows that the poles for the symmetric states are to be determined from

$$\begin{aligned} & \left(i \sin \theta_1 - \frac{k_1}{q_1} \cos \theta_1 \right) \left(\sin \theta_2 - \frac{|k_2|}{q_2} \cos \theta_2 \right) \\ &= \eta \left(i \sin \theta_2 - \frac{k_1}{q_2} \cos \theta_2 \right) \left(\sin \theta_1 - \frac{|k_2|}{q_1} \cos \theta_1 \right), \end{aligned} \quad (28)$$

where $\eta \equiv U_{12}^2/(U_{11}U_{22})$ is the coupling parameter of two interfering channels. In the decoupling limit, $U_{12} = 0$, Eq. (28) defines the bound-state levels ($\equiv E_B$) in the well through

$$\tan \theta_2 = \frac{|k_2|}{q_2}. \quad (29)$$

In the weak-coupling limit, we have obtained the poles $E_p = E_R - i\Gamma$ to the first order in η as

$$E_R = E_B + \eta E_R^{(1)} \quad \text{and} \quad \Gamma = \eta \Gamma^{(1)}, \quad (30)$$

where

$$E_R^{(1)} = 4 \frac{(E_B - E_2^*)|k_2|(|k_2|\cos \theta_1 - q_1 \sin \theta_1)(k_1^2 \cos \theta_1 + q_1|k_2|\sin \theta_1)}{(|k_2|L_a + 2)(q_2^2 + |k_2|^2)(k_1^2 \cos^2 \theta_1 + q_1^2 \sin^2 \theta_1)}$$

and

$$\Gamma^{(1)} = 4 \frac{(E_B - E_2^*)|k_2|k_1(|k_2|\cos \theta_1 - q_1 \sin \theta_1)^2}{(|k_2|L_a + 2)(q_2^2 + |k_2|^2)(k_1^2 \cos^2 \theta_1 + q_1^2 \sin^2 \theta_1)}.$$

Similarly, the zero energies from the symmetric states are estimated to the lowest order in η as

$$E_0 = E_B + \eta E_0^{(1)} \quad (31)$$

by solving

$$\left(\sin \theta_2 - \frac{|k_2|}{q_2} \cos \theta_2 \right) \left(\sin \theta_2 + \frac{q_2}{|k_2|} \cos \theta_2 \right) = \frac{U_{11}}{U_{22}} \eta \left(\sin \theta_1 - \frac{|k_2|}{q_1} \cos \theta_1 \right) \left(\sin \theta_1 + \frac{q_1}{|k_2|} \cos \theta_1 \right), \quad (32)$$

perturbatively, that is two-channel approximation of Eq. (18). The correction to zero energy $E_0^{(1)}$ is given by

$$E_0^{(1)} = 4 \frac{U_{11}}{U_{22}} \frac{(E_B - E_2^{tr}) |k_2|^2 (|k_2|/q_1 \cos \theta_1 - \sin \theta_1) (q_1/|k_2| \cos \theta_1 + \sin \theta_1)}{(|k_2|L_a + 2)(q_2^2 + |k_2|^2)}.$$

Equations (30) and (31) are the desired analytical expressions for the resonance poles and zero energies that describe the Fano structures, numerically seen in Figs. 2–4.

One can quickly notice that the width of resonance peak may shrink to zero, $\Gamma \rightarrow 0$, for

$$\tan \theta_1 = \frac{|k_2|}{q_1}. \quad (33)$$

Importantly, when this happens $E_R^{(1)}$ and $E_0^{(1)}$ also vanish identically: the complex poles and real zero energies in Eq. (25) approach to the common real energies, $E_p, E_0 \rightarrow E_c$ to give $t_{11}(E_c) = 1$. Thus, the very real energies at which the collapse of Fano structures occur, for instance $E_c = 3.255 E_1$ in Fig. 3(c), are to be specified by solving Eqs. (29) and (33) simultaneously. [We have confirmed that, in general, the critical states are defined by the simultaneous solutions to Eqs. (17) and (18).] We solved this *two spectral-variable problem* by choosing energy E and distance L_a as the relevant variables. The rest of the system parameters such as the impurity strength etc. are assumed to be given. By manipulating Eqs. (29) and (33) one can obtain the spectral variables as

$$E_c(j) = E_2^{tr} + (E_2 - E_2^{tr}) \cos^2 \alpha(j), \quad (34)$$

$$L_c(j) = \frac{2}{\pi} \frac{W \alpha(j)}{\cos \alpha(j)} \left(\frac{E_1}{E_2 - E_2^{tr}} \right)^{1/2}, \quad (35)$$

where $j = 1, 2, \dots$ and the parameters $\alpha(j)$ are to be specified by the transcendental equation

$$f(\alpha) = \sqrt{\epsilon + \cos^2 \alpha} \tan \left(\frac{\alpha}{\cos \alpha} \sqrt{\epsilon + \cos^2 \alpha} \right) - \sin \alpha = 0, \quad (36)$$

where $\epsilon \equiv (E_2 - E_1)/(E_2 - E_2^{tr})$. Its solution restricts that $0 < \alpha(j) \leq \pi/2$. When the obtained $\alpha(j)$ are substituted into Eqs. (34) and (35), the *critical* energies and impurity sizes are determined. We report a few of the critical values in Table I. The corresponding wave functions to the critical scattering states are given as

$$\Psi(x, y) = A_1 e^{ik_1(x + L_a/2)} \varphi_1(y), \quad (37)$$

for $x \leq -L_a/2$,

$$\begin{aligned} \Psi(x, y) = & A_1 U_{11} \left[\cos(q_1 x + \theta_1) + i \frac{k_1}{q_1} \sin(q_1 x + \theta_1) \right] \chi_1(y) \\ & + A_1 U_{12} \left[\cos(q_2 x + \theta_2) + i \frac{k_1}{q_2} \sin(q_2 x + \theta_2) \right] \chi_2(y), \end{aligned} \quad (38)$$

for $-L_a/2 \leq x \leq L_a/2$, and

$$\Psi(x, y) = A_1 e^{ik_1(x - L_a/2)} \varphi_1(y), \quad (39)$$

for $x \geq L_a/2$. The wave functions clearly manifest that the full transmission occurs without reflection at the critical energies, i.e., $T(E_c) = 1$: the incident current density comes fully out of the impurity region.

The inversion of the resonance peak and transmission zero observed in Fig. 3 can be accounted for as follows. From Eqs. (30) and (31) we have estimated that the relative displacement between the adjacent Fano peak and zero energy, i.e., $E_R - E_0$, behaves as $\sim (\tan \theta_1 - |k_2|/q_1) g(E, L_a; \eta)$ [the function g is rather complicated, accordingly whose explicit form is not given here]. What is relevant is the fact that as E and L_a are tuned to the critical values, $E_R - E_0$ vanishes identically and it reverses its sign before and after this takes places. Similar inversion of the resonance levels was discussed, for instance by Tekman and Bagwell in Ref. 13, however, the origin of the phenomenon is different. In Tekman and Bagwell's work such a phenomenon was predicted because they changed the impurity model potential from an attractive one to a repulsive one. This caused the sign change in the interchannel transition-matrix element, which in turn switched the role of the constructive and destructive interference between the involved channels. It is important to note that in our case the inversion of the resonance levels is the purely coherent effect originated by the change of the spatial extension of the attractive impurity along the electron propagation direction.

Next, we investigate the phase information of the transmissivity. Near a Fano resonance structure the phase shift associated with the transmission amplitude is given by

$$\tan \delta = \frac{\Gamma}{E_R - E}. \quad (40)$$

We depict this in Fig. 5 for the same parameters used in Fig. 3. In Fig. 5(a), the phase remains zero for most of the energies below the resonance peak, but it increases rapidly to the value of $\pi/2$ as the energy approaches the zero energy. After the energy passes through the transmission zero, the phase

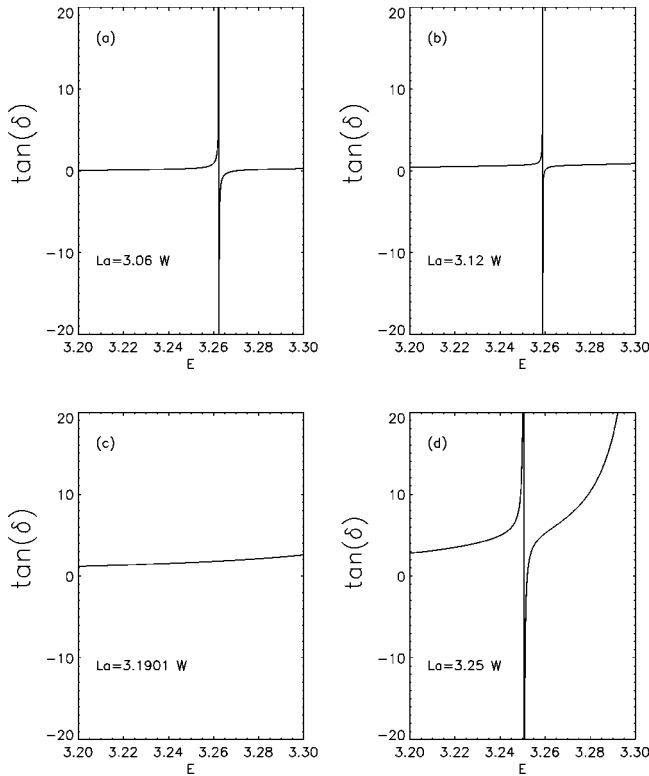


FIG. 5. Phase of the transmission amplitude near a Fano resonance as a function of the energy E , where all the parameters used are the same as in Fig. 3.

changes its sign abruptly to become $-\pi/2$. Then, it remains negative and increases sharply to become zero. Similar behavior is seen in Fig. 5(b) with the impurity size closer to the critical value, where the phase change $\pi/2 \rightarrow -\pi/2$ near the resonance becomes even more abrupt. When the impurity size L_a is at the critical value in Fig. 5(c), the phase remains nearly constant, corresponding to Fig. 3(c) where the Fano resonances collapse. After the resonance-level inversion in Fig. 3(d), the similar behavior to Figs. 5(a) and 5(b) is recovered in Fig. 5(d) except for a dramatic rise to positive phase for energies larger than resonance energy, a consequence of the influence of other Fano resonances at higher energies. The distinctive nature of Fig. 5(c) again manifests the formation of a critical scattering state from the resonance states. The flatness of the phase in energy, $d\delta(E)/dE \sim 0$, is connected with no space-charge accumulation in the local electron density as studied in Ref. 23. This is evident in our obtained electron wave functions, Eqs. (37)–(39).

V. ELECTRON CONFINEMENT

The critical states obtained deserve particular attention. Very interestingly, we have found that the critical states are degenerated in energy. There exist two independent configurations, possessing the same energies: one is the scattering configuration that we have discussed so far and the other is the one related to the electron confinement. The electron-confinement configuration can be understood as follows. The spatial region occupied by the finite-size impurity resembles the Fabry-Perot resonator in optics,²⁴ where two edges of the attractive well play the role as electronic *mirrors*, for the

electron waves. Equations (29) and (33) define the real solutions to the Fabry-Perot resonance condition for two interfering waves in the resonator. The conditions are equivalent to having solutions to the Schrödinger equation Eq. (2) for an electron injected into the well region with the boundary conditions, $\psi_c \rightarrow 0$ as $x \rightarrow \pm\infty$. For the symmetric states considered, the solutions are

$$\Psi_c(x, y) = c_1 \cos(q_1 x) \chi_1(y) + c_2 \cos(q_2 x) \chi_2(y), \quad (41)$$

for $|x| < L_a/2$ and

$$\Psi_c(x, y) = C_1 e^{-|k_2|(x-L_a/2)} \varphi_2(y), \quad (42)$$

for $x > L_a/2$. Thus, the allowed critical states also correspond to the discrete levels embedded in the continuum, describing the *localized* electron states over the well region. These localized states are to be distinguished from the bound levels calculated from Eq. (29) that defines the bound-state solutions to a square-well potential with depth $E_2 - E_2^{tr}$ and width L_a .²⁵ The bound levels E_B are rather fictitious because they are the ideal solutions obtained strictly in the decoupling limit among the participating channels. On the other hand, the localized wave functions Eqs. (41) and (42) take into account the physical channel mixing caused by the impurity scattering and are consequences of the coherent interaction of two interfering channels in the finite space over the impurity. They are very special solutions to the Schrödinger equation via the Fabry-Perot mechanism under the multichannel conditions. When the impurity size is off-tuned from the critical values, Eqs. (29) and (33) or in general Eqs. (17) and (18) do not admit the simultaneous, real solutions. Then, the system allows only the complex solutions specifying resonances states and the electron-confinement is not possible. One way to confirm the formation of the long-living electron states predicted in the quantum waveguide would be to use scanning tunneling microscopy. Since those electrons injected with the critical energies will be trapped in the impurity with the corresponding critical sizes, a dip in the tunneling current should be signaled. The prediction of the peculiar degeneracy of the scattering states, Eqs. (37)–(39), with the localized states, Eqs. (41)–(42), seems very interesting in nanostructure, and these kinds of quantum states in atomic systems were discussed in the literature.²⁶ Although we have reported our analysis only on the symmetric states, we carried out a similar analysis for the antisymmetric states as well. The similar electron confinement problem in nanostructures has been reported under the time-dependent situation.²⁷

VI. CONCLUSION

We have investigated the electron transmission through the Q1D quantum waveguide that contains a finite-size attractive impurity. The analysis was performed using a formally exact formulation for the scattering matrix as a function of the electron energy while varying the impurity parameters. Consequently, we have obtained the various interesting coherent resonance effects due to the multi-impurity levels and the geometrical extension of the finite-size attractive scatterer under the many-channel condition.

Our calculation predicts very interesting new coherent effects in the electron transmission problem through narrow constrictions. It was possible to generate two distinctive

types of resonance structures, the Breit-Wigner resonances and the Fano line shapes in the same energy window considered. They interact in a complicated fashion as the system parameters are changed and the Fano resonance dominates when the two overlap. We have observed that the Fano resonance level is inverted as the impurity size is changed. Also, the Fano resonance and antiresonance collapse at the critical energies and the critical impurity sizes, and the full transmission takes place at such a critical state. We have shown that the collapse of the Fano resonances also corresponds to the occurrence of very special localized electron states, i.e., the appearance of discrete levels in the continuum. The obtained mechanism may be used to localize electrons in the region of interest in the quantum waveguide.

Some of the coherent effects studied in this paper should be observable in high-mobility nanostructures at low temperatures, for instance in a typical Q1D nanochannel made of GaAs/Al_xGa_{1-x}As heterostructures. An artificial finite-size impurity may be created in the quantum waveguide using recent nanotechnology.²⁸

ACKNOWLEDGMENTS

We would like to thank P. J. Price for calling our attention to the inversion of resonance level and for providing us with useful comments. We also thank H.-W. Lee for a careful reading of the manuscript. This work was supported by the CNU Research Fund and also in part by the Ministry of Education of Korea through Grant No. BSRI-98-2431. A.M.S. acknowledges support from the Russian Basic Research Foundation, Grant No. 97-02-169231. One of the authors (Y.S.J.) acknowledges partial support by the Research Fellows Program of the Center for Energy Research/Education/Service at Ball State University.

APPENDIX A: SHORT-RANGE IMPURITY MODEL

In this Appendix, we present a limiting case of our finite-size impurity model, namely an extremely short-ranged impurity along the propagation direction but having the lateral extension. This model was treated in Ref. 13 using a two-band model in the energy window defined by the bottom of the lowest and next subband. Recently, an additional analysis was reported in an extended energy window with incorporating three subbands.²⁰ Such a thin impurity model can be achieved from our more general model by assuming that the longitudinal size of the impurity L_a is much less than the characteristic wavelengths of the electron,

$$L_a \ll q_n^{-1} \ll k_n^{-1}, \quad (\text{A1})$$

but no restriction is given to the transverse extension W_a .²⁹ By expanding Eq. (16) in terms of $L_a q_n$, one can find

$$\mathbf{M} = (i\mathbf{k})^{-1}(i\mathbf{k} + \mathbf{v}), \quad (\text{A2})$$

where $\mathbf{v} \equiv \frac{1}{2}L_a \mathbf{U}^{-1} \mathbf{q}^2 \mathbf{U}$, whose matrix elements $(\mathbf{v})_{nn'} \equiv v_{nn'}$ are given in Ref. 20.

In addition to the restriction Eq. (A1), we impose the weak-coupling approximation for a simple analytical treatment,

$$\frac{\hbar^2}{2m^*} v_{nn'}^2 \ll |E_n - E_{n'}|, \quad (\text{A3})$$

where $|E_n - E_{n'}|$ is the energy spacing between two nonidentical subbands. This approximation has been motivated by the fact that the matrix elements $v_{nn'}$ are decreasing functions of $|n - n'|$. Accordingly, for a chosen energy near E_n only a small number of subbands are involved in calculating electron transmission, validating use of the *finite channel approximation*. In other words, a perturbative analysis of Eq. (A2) is possible in this case. Keeping only the diagonal matrix elements for interaction matrix elements in Eq. (A2) as the lowest order treatment, we get from Eq. (15)

$$t_{nn}(E) = \frac{ik_n}{ik_n + v_{nn}}. \quad (\text{A4})$$

The poles $\mathcal{E}^{(0)}$ to Eq. (A4) are real and define the bound-state levels as

$$\mathcal{E}_n^{(0)} = E_n - \frac{\hbar^2 v_{nn}^2}{2m^*}. \quad (\text{A5})$$

Corrections to these levels come for the mixing of the channels. For an incident energy E near $\mathcal{E}_2^{(0)}$ in the energy window (E_1, E_2) , it suffices to consider only a two-channel approximation in the weak-coupling limit. In this case, the transmission is solely determined by the amplitude $t_{11}(E)$ because only $n=1$ is the propagating channel. The result has been obtained by Eqs. (15) and (A2) as

$$t_{11}(E) = \frac{ik_1}{ik_1 + v_{11} - v_{12}[1/(ik_2 + v_{22})]v_{21}}. \quad (\text{A6})$$

The amplitude $t_{11}(E)$ possesses a pole at

$$E_p = E_R - i\Gamma, \quad (\text{A7})$$

where

$$E_R \approx \mathcal{E}_2^{(0)} + \frac{\hbar^2 v_{11} v_{22} v_{12}^2}{m^*(k_1^2 + v_{11}^2)} \quad \text{and} \quad \Gamma \approx \frac{\hbar^2 k_1 v_{12}^2 v_{22}}{m^*(k_1^2 + v_{11}^2)}.$$

Also, we found that the amplitude $t_{11}(E)$ vanishes identically at zero energy

$$E_0 = \mathcal{E}_2^{(0)}. \quad (\text{A8})$$

We see that the pole and the zero energy are situated close to each other in the complex energy plane. Then, it is possible to write the transmission amplitude in the neighborhood of a resonance in the form given in Eq. (25) in the text. Equation (A6) is identical to Eq. (3.2) in Ref. 13 with $v_{nn'} = 2V_{nn'}$. But, by writing the transmission amplitude $t_{11}(E)$ in this way, it becomes clear to understand that the evanescent mode $n=2$ plays a role as a *virtual* channel for electron transmission.

Note that for $W_a/W \ll 1$, the interchannel matrix elements $v_{nn'}$ tend to

$$v_{nn'} = \gamma \varphi_n(Y_c) \varphi_{n'}(Y_c), \quad (\text{A9})$$

where $\gamma \equiv (m^*/\hbar^2)V_{att}L_aW_a$, which corresponds to the point-impurity model studied in Ref. 6. In this case, there is an additional relation among the matrix elements as $v_{11}v_{22} = v_{12}v_{21}$. Due to this relation one can confirm from Eq. (A6) that $t_{11}(E_2)$ equals unity, i.e., the full transmission occurs at the subband minimum E_2 and the Fano dip remains at the

same zero energy $\mathcal{E}_2^{(0)}$. This is the characteristic of the isotropic scattering center, that has been discussed in Refs. 4 and 6. Our calculation with the lateral extension shows that the effect of an anisotropic scatterer on the transmission is to displace the location of the perfect transmission down to the bottom of subbands.²⁰

-
- ¹B.J. van Wees, H. van Houten, C.W.J. Beenakker, J.G. Williamson, L.P. Kouwenhoven, D. van der Marel, and C.T. Foxon, *Phys. Rev. Lett.* **60**, 848 (1988).
- ²D.A. Wharam, T.J. Thornton, R. Newbury, M. Pepper, H. Ahmed, J.E.F. Frost, D.G. Hasko, D.C. Peacock, D.A. Ritchie, and G.A.C. Jones, *J. Phys. C* **21**, L209 (1988).
- ³*Nanostructure Physics and Fabrication*, edited by M. A. Reed and W. P. Kirk (Academic, Boston, 1989).
- ⁴C.S. Chu and R.S. Sorbello, *Phys. Rev. B* **40**, 5941 (1989).
- ⁵P.L. McEuen, B.M. Alphenaar, R.G. Weeler, and R.N. Sack, *Surf. Sci.* **229**, 312 (1990).
- ⁶P.F. Bagwell, *Phys. Rev. B* **41**, 10 354 (1990); *J. Phys.: Condens. Matter* **2**, 6179 (1990).
- ⁷J. Faist, P. Guéret, and H. Rothuizen, *Phys. Rev. B* **42**, 3217 (1990).
- ⁸E. Tekman and S. Ciraci, *Phys. Rev. B* **42**, 9098 (1990).
- ⁹M.W. Dellow, P.H. Beton, C.J.G. Langerak, T.J. Foster, P.C. Main, L. Eavas, H. Henimi, S.P. Beamont, and C.D. Wilkinson, *Phys. Rev. Lett.* **68**, 1754 (1992).
- ¹⁰Ch. Kunze and R. Lenk, *Solid State Commun.* **84**, 457 (1992).
- ¹¹C.C. Eugster, J.A. del Alamo, M.R. Melloch, and M.J. Rooks, *Phys. Rev. B* **46**, 10 146 (1992).
- ¹²Y.B. Levinson, M.I. Lubin, and E.V. Sukhorukov, *Phys. Rev. B* **45**, 11 936 (1992); S.A. Gurvitz and Y.B. Levinson, *ibid.* **47**, 10 578 (1993).
- ¹³E. Tekman and P.F. Bagwell, *Phys. Rev. B* **48**, 2553 (1993).
- ¹⁴P.J. Price, *Phys. Rev. B* **48**, 17 301 (1993).
- ¹⁵J.U. Nöckel and A.D. Stone, *Phys. Rev. B* **50**, 17 415 (1994).
- ¹⁶A. Mosk, Th.M. Nieuwenhuizen, and C. Barnes, *Phys. Rev. B* **53**, 15 914 (1996).
- ¹⁷Y.S. Joe and R.M. Cosby, *J. Appl. Phys.* **81**, 6217 (1997); *Solid State Commun.* **101**, 731 (1997).
- ¹⁸R. Landauer, *Philos. Mag.* **21**, 863 (1970).
- ¹⁹M. Büttiker, *Phys. Rev. B* **35**, 4123 (1987).
- ²⁰C.S. Kim and A.M. Satanin, *Zh. Éksp. Teor. Fiz.* **115**, 211 (1999) [*JETP* **88**, 118 (1999)].
- ²¹U. Fano, *Phys. Rev.* **104**, 1866 (1961).
- ²²F.H. Mies, *Phys. Rev.* **175**, 164 (1968).
- ²³P.J. Price, *Superlattices Microstruct.* **20**, 253 (1996).
- ²⁴M. Born and E. Wolf, *Principles of Optics* (Cambridge, Cambridge, 1997).
- ²⁵J. J. Sakurai, *Modern Quantum Mechanics* (Benjamin/Cummings, Menlo Park, CA, 1985), p. 451.
- ²⁶For instance, see J. von Neumann and E. Wigner, *Z. Phys.* **30**, 465 (1929); L. Fonda and R.G. Newton, *Ann. Phys. (N.Y.)* **10**, 490 (1960); F.H. Stillinger and D.R. Herrick, *Phys. Rev. A* **11**, 446 (1975); H. Friedrich and D. Wintgen, *ibid.* **31**, 3964 (1985).
- ²⁷C.S. Kim and A.M. Satanin, *Phys. Rev. B* **58**, 15 389 (1998); *J. Phys.: Condens. Matter* **10**, 10 587 (1998).
- ²⁸S. Yamada and M. Yamamoto, *J. Appl. Phys.* **79**, 8391 (1996).
- ²⁹This situation corresponds to the extremely localized impurity along the propagation direction where we impose $L_a \rightarrow 0$ and $V_{att} \rightarrow \infty$ with holding $L_a V_{att} = \text{const}$. In this limit, q_n behaves as $\sim \sqrt{2m^*V_{att}/\hbar^2} \ll k_n$, accordingly, $L_a q_n^2 \sim \text{const}$.